Journal of Magnetism and Magnetic Materials 456 (2018) 142–149

Contents lists available at ScienceDirect

Journal of Magnetism and Magnetic Materials

journal homepage: www.elsevier.com/locate/jmmm

Research articles

Quasi-one-dimensional magnetism in $Mn_xFe_{1-x}Nb_2O_6$ compounds: From Heisenberg to Ising chains

M.L. Hneda [a,c,d], S.R. Oliveira Neto [b,c], J.B.M. da Cunha [a], M.A. Gusmão [a], O. Isnard [c,d,*]

[a] Universidade Federal do Rio Grande do Sul, CP 15051, 91501-970 Porto Alegre, Brazil
[b] Universidade Federal de Sergipe, 49100-000 São Cristóvão, Brazil
[c] CNRS, Institut Néel, 25 rue des Martyrs, BP 166, F-38042 Grenoble, France
[d] Université Grenoble Alpes, Institut Néel, F-38042 Grenoble, France

ARTICLE INFO

Article history:
Received 3 October 2017
Received in revised form 5 January 2018
Accepted 4 February 2018
Available online 5 February 2018

Keywords:
Low-dimensional magnetism
Neutron diffraction
Heisenberg and Ising chains

ABSTRACT

A series of $Mn_xFe_{1-x}Nb_2O_6$ compounds ($0 \leqslant x \leqslant 1$) is investigated by both X-ray and neutron powder diffraction, as well as specific-heat and magnetic measurements. The samples present orthorhombic *Pbcn* crystal symmetry, and exhibit weakly coupled magnetic chains. These chains are of Heisenberg type (weak anisotropy) on the Mn-rich side, and Ising-like (strong anisotropy) on the Fe-rich side. Except for 100% Fe ($x = 0$), which has weakly-interacting ferromagnetic Ising chains, a negative Curie-Weiss temperature is obtained from the magnetic susceptibility, indicating dominant antiferromagnetic interactions. At the lowest probed temperature, $T = 1.5$ K, true long-range magnetic order is only observed for $x = 1$, 0.8, and 0. Although the ordering is globally antiferromagnetic in all cases, the first two are characterized by a two-sublattice structure with propagation vector $\mathbf{k} = (0, 0, 0)$, while the latter presents alternatingly oriented ferromagnetic chains described by $\mathbf{k} = (0, \frac{1}{2}, 0)$. For other compositions, short-range magnetic correlations are extracted from diffuse neutron-scattering data.

1. Introduction

Columbite materials have a common formula ANb_2O_6 (A = Fe, Mn, Co, Ni, Zn), with orthorhombic structure of the *Pbcn* space group [1–3]. These materials belong to the AB_2O_6 family, which has been extensively studied because of interesting photoluminescence [4] and dielectric [5,6] properties, but particularly attractive for their remarkable magnetic properties [1,7,8]. The crystal structure depends strongly on the B ion nature. For example, B = Ta yields a tetragonal structure [7], Nb favors an orthorhombic one [1,2], while monoclinic and triclinic structures are observed with V [9,10]. According to Blasse [11], these differences occur due to covalence and polarization effects in B^{5+}-O^{2-}-B^{5+} configurations, brought about by delocalization of oxygen electrons depending on the type of the nearby metal cation B^{5+}.

We have recently reported [7,12–14] results on the ANb_2O_6 and ATa_2O_6 series of compounds, characterized by 1D and 2D magnetic behavior, respectively. The ANb_2O_6 phases exhibit weakly interacting one-dimensional magnetic chains [1,15,16]. $MnNb_2O_6$ was found to undergo a transition from a paramagnetic phase to an ordered structure [2,17,18] at 4.40 K, while an ordering temperature of 5.5 K has been reported for $FeNb_2O_6$ [3,19]. An interesting quantum-critical behavior has been reported for $CoNb_2O_6$ [20], triggering a renewed interest of the scientific community [21–24] on experimental realization and new properties of transverse-field Ising systems.

Our group has worked mainly on systems with mixture of cations in the A site in order to understand which crystallographic and magnetic parameters play a fundamental role for the determination of the magnetic structure. All the Nb compounds, with Co^{2+}, Fe^{2+}, Ni^{2+} cations in the octahedral A site, form ferromagnetic zig-zag chains along the c-axis, with a triangular-lattice arrangement of the chains in the basal ab plane. Following these earlier studies, in this work we investigate how crystallographic and magnetic properties of the series $Mn_xFe_{1-x}Nb_2O_6$ evolve as function of the relative concentrations of the magnetic ions. This is a novel situation since Mn^{2+} is known to prefer AF magnetic coupling along the chains [16], in contrast to the preference of Fe to form ferromagnetic chains [14]. Using XAS spectroscopy, Tarantino et al. [25] have recently reported on the local structural properties of $(Mn, Fe)Nb_2O_6$ around the Fe and Mn cations. Here we present a systematic study of structural and magnetic properties of the $(Mn, Fe)Nb_2O_6$ series, using X-ray (XRD) and neutron powder

* Corresponding author at:.
E-mail address: olivier.isnard@grenoble.cnrs.fr (O. Isnard).

https://doi.org/10.1016/j.jmmm.2018.02.011
0304-8853/

diffraction (ND), complemented by magnetization, susceptibility, and specific-heat measurements.

2. Experimental details

Samples of $Mn_xFe_{1-x}Nb_2O_6$ were prepared for $x = 0.0$, 0.2, 0.4, 0.5, 0.6, 0.8, and 1.0, with appropriate amounts of Mn acetate ($C_4H_6MnO_4 \cdot 4H_2O$), MnO, Fe_2O_3, Nb_2O_5, and metallic Fe. $MnNb_2O_6$ was subjected to heat treatments in air, at 400, 650, 725 and 1100 °C for 12, 16, 48 and 36 h respectively. Stoichiometric mixtures containing Fe were ground, pressed into pellets, and heat-treated in vacuum at 1100 °C for 24 h. Sample purity was first checked by X-ray-diffraction (XRD) analysis at room temperature. This was done in Bragg-Brentano geometry, using Cu Kα radiation, $\lambda(K_{\alpha 1}) = 1.5406$ Å and $\lambda(K_{\alpha 2}) = 1.5444$ Å, with a scan step of 0.05° and angular 2θ range from 10° to 90°.

ND patterns were recorded with the double-axis high-flux diffractometer D1B. This is a powder diffractometer operating with a take-off angle of the monochromator of 44° (in 2θ). In this configuration the multicounter is composed of 1280 cells covering a total angular domain of 128° (in 2θ), with a detector step of 0.1°. This line is operated by the CNRS at the Institut Laue Langevin (ILL), Grenoble, using a 2.52 Å wavelength selected by a pyrolytic graphite monochromator. A vanadium sample holder was used.

Rietveld refinement with the FULLPROF package [26] was used to extract the crystallographic and magnetic parameters from XRD and ND data. Agreement factors used in this procedure are defined according to the guidelines of the Rietveld refinement [27].

Magnetization measurements were undertaken on powder samples in the temperature range from 1.9 to 300 K, using an extraction magnetometer. Isothermal magnetization curves were recorded in applied magnetic fields ranging from $\mu_0 H = 0$ to 10 T, and the thermal dependence of the magnetic susceptibility was determined through magnetization measurements in a field of 0.5 T.

Specific-heat was measured on pellets (mass ~5 mg), with the temperature relaxation method in the range of 1.8–300 K, using a PPMS (Physical Property Measurement System – Quantum Design). This method consists in increasing the sample temperature with a known power, and then fitting the temperature relaxation during heating and cooling.

3. Results and discussion

3.1. X-ray diffraction

From XRD-pattern analysis we observe that all the $Mn_xFe_{1-x}Nb_2O_6$ samples present a single phase with the *Pbcn* space-group symmetry. An example of Rietveld analysis of the X-ray pattern recorded at room temperature is shown in Fig. 1 for $x = 0.5$. Fig. 2 shows the concentration dependence of the unit-cell parameters for the series. A small (1% or less) anisotropic expansion was observed in the cell parameters between the end-member compounds ($x = 0$ and 1): $\Delta a/a = 0.0110$, $\Delta b/b = 0.0046$ and $\Delta c/c = 0.0059$. The room-temperature atomic positions, cell parameters, and Rietveld agreement factors are summarized in Table 1.

3.2. Magnetic measurements

Temperature dependence of the dc magnetic susceptibility for $Mn_xFe_{1-x}Nb_2O_6$ samples recorded at $\mu_0 H = 0.5$ T is shown in Fig. 3(a). The characteristic susceptibility curves for this type of low-dimensional compounds present a broad peak, and the ordering temperature corresponds to an inflection point some degrees

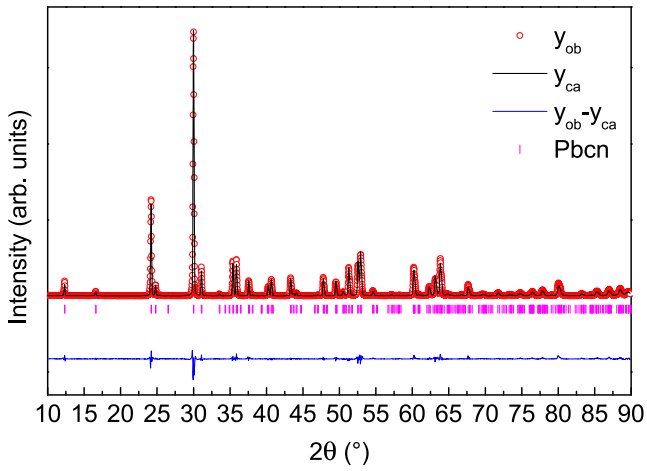

Fig. 1. Rietveld refinement of the X-ray diffraction pattern recorded at room temperature for $Mn_{0.5}Fe_{0.5}Nb_2O_6$. The Bragg positions correspond to the *Pbcn* space group, as indicated.

below the maximum. This inflection point can be better located as a peak in the thermal derivative $\partial(T\chi)/\partial T$, as shown in the inset of Fig. 3(b) for the end-members of the series ($x = 0$ and 1). Only the compounds with $x = 0$, 0.8, and 1 exhibit a long-range ordering transition in the measuring temperature range ($1.9\ K \leqslant T \leqslant 300\ K$).

The paramagnetic susceptibility as a function of temperature was fitted to the Curie-Weiss law, $\chi(T) = C/(T - \theta_{CW})$ for temperatures typically above 50 K. To illustrate this procedure, Fig. 4 presents a fitting of $1/\chi$ for $Mn_{0.5}Fe_{0.5}Nb_2O_6$. This is, in fact, a peculiar case, in that the inverse susceptibility drops below the Curie-Weiss straight line, which probably indicates a ferrimagnetic behavior at this composition. Values of the effective magnetic moment in the paramagnetic state can be obtained from the fitted Curie constant C as $\mu_{\text{eff}} = (3 k_B C/N_A)^{1/2} \mu_B$, where N_A is the Avogadro's number.

Table 2 shows the parameters obtained from this analysis, for all samples. There we can see that there is no long-range ordering for x = 0.2, 0.4, 0.5, and 0.6. Suppression of magnetic ordering has also been reported for intermediate compositions of $Ni_xFe_{1-x}Nb_2O_6$ and $Fe_xCo_{1-x}Nb_2O_6$ compounds [12,14] at least for temperatures of 2 K or above. The values of Curie-law parameters quoted in Table 2 for $MnNb_2O_6$ are also in agreement with those reported in Ref. [28] ($\theta_{CW} = -20.5$ K, $C = 4.37$ emu K/mol Oe, and $\mu_{\text{eff}} = 5.91\mu_B$).

In an octahedral oxygen environment, 3d-metal cations are expected to be in a high-spin state, which means $S = 5/2$ for Mn^{2+} and $S = 2$ for Fe^{2+}. The theoretical effective magnetic moment of Mn^{2+} supposing pure-spin contribution ($g = 2$) is $5.92\mu_B$. This value is close to the one obtained from susceptibility measurements, quoted in Table 2, but a small orbital effect cannot be ruled out. This is also seen in Fig. 5, where experimental values of the fitted magnetic moment for $Mn_xFe_{1-x}Nb_2O_6$ compounds are plotted in comparison with the spin-only prediction for the composition-averaged cation spin. There we can see that orbital effects become more noticeable for higher Fe content. Although only Mn has $L = 0$ in the ground-state, one should expect crystal-field effects to yield quenching of the angular momentum also for Fe. The observed differences reflect second-order orbital corrections to the g-factor, including anisotropy, since $FeNb_2O_6$ is well described by an Ising model [14].

Fig. 6(a) shows isothermal magnetization curves recorded at 2 K for all the samples under study. $FeNb_2O_6$ undergoes a metamagnetic transition around $\mu_0 H = 1$ T. This is consistent with an over-

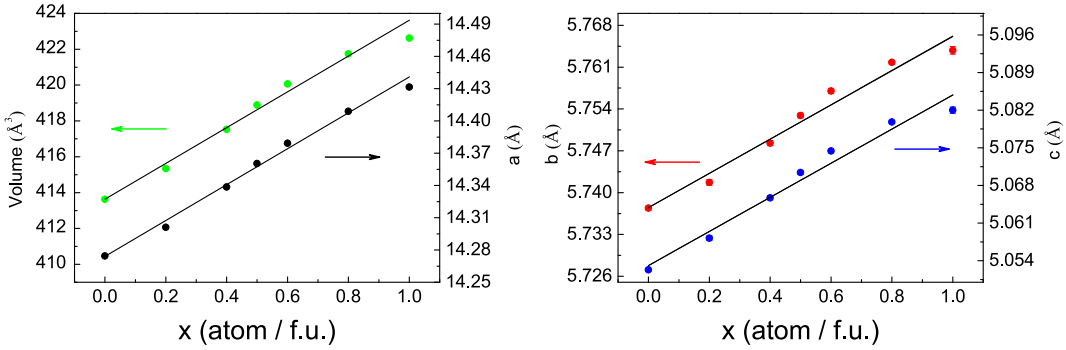

Fig. 2. Composition dependence of the unit-cell volume and lattice parameters in the $Mn_xFe_{1-x}Nb_2O_6$ compounds.

Table 1
Structural parameters obtained from X-ray powder diffraction at room temperature for $Mn_xFe_{1-x}Nb_2O_6$ compounds.

x	→	0.0	0.2	0.4	0.5	0.6	0.8	1.0
	x	0	0	0	0	0	0	0
Mn/Fe	*y*	0.169(2)	0.170(2)	0.174(2)	0.174(2)	0.172(2)	0.176(2)	0.180(3)
	z	0.25	0.25	0.25	0.25	0.25	0.25	0.25
	x	0.1602(3)	0.1615(3)	0.1618(2)	0.1620(2)	0.1621(2)	0.1622(2)	0.1626(3)
Nb	y	0.319(7)	0.3187(6)	0.3199(5)	0.3196(5)	0.3192(6)	0.3191(5)	0.3188(9)
	z	0.750(2)	0.750(2)	0.754(1)	0.753(1)	0.755(1)	0.7568(9)	0.760(2)
	x	0.108(1)	0.099(1)	0.099(1)	0.097(1)	0.099(1)	0.099(1)	0.102(2)
O1	*y*	0.400(5)	0.408(4)	0.406(3)	0.405(3)	0.408(4)	0.408(3)	0.412(5)
	z	0.424(7)	0.429(6)	0.426(4)	0.427(4)	0.447(5)	0.443(4)	0.445(7)
	x	0.085(1)	0.080(1)	0.082(1)	0.081(1)	0.084(1)	0.083(1)	0.083(2)
O2	*y*	0.112(5)	0.123(5)	0.116(4)	0.118(4)	0.125(4)	0.122(3)	0.127(6)
	z	0.912(7)	0.899(6)	0.905(4)	0.905(4)	0.892(5)	0.894(4)	0.888(7)
	x	0.266(2)	0.255(2)	0.257(2)	0.255(2)	0.254(2)	0.255(2)	0.253(3)
O3	*y*	0.127(5)	0.122(4)	0.129(3)	0.127(3)	0.126(4)	0.125(3)	0.127(6)
	z	0.585(7)	0.578(5)	0.583(4)	0.586(4)	0.587(5)	0.585(4)	0.586(6)
a (Å)		14.2743(6)	14.3011(9)	14.338(4)	14.3602(7)	14.3792(7)	14.409(0)	14.431(1)
b (Å)		5.7374(2)	5.7416(3)	5.748(2)	5.7529(3)	5.7569(3)	5.761(8)	5.7638(4)
c (Å)		5.0522(2)	5.0582(3)	5.065(7)	5.0704(2)	5.0744(2)	5.0798(3)	5.0820(4)
Volume (Å^3)		413.77(3)	415.34(4)	17.5(2)	418.88(3)	420.06(3)	421.7(4)	422.73(5)
R_{wp} (%)		21.3	18.2	14.2	14.4	17.6	14.9	15.2
R_B (%)		10.4	4.7	4.5	5.7	4.5	3.5	4.8

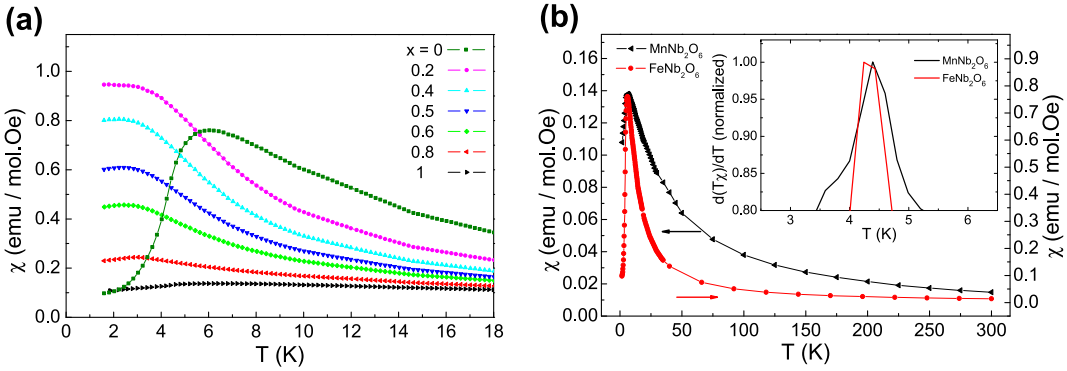

Fig. 3. (a) Temperature dependence of the dc susceptibility recorded at μ_0 H = 0.5 T for $Mn_xFe_{1-x}Nb_2O_6$ samples and (b) a comparison between the end compounds of the series (x = 0 and 1); the inset shows the derivative $\partial(T\chi)/\partial T$, whose maximum determines T_N.

all AF ordering resulting from alternatingly oriented FM chains, observed for ANb_2O_6 systems, with A = Fe, Co, and Ni [12,14]. A relatively low magnetic field overcomes the weak interchain AF interaction, and a spin-flip transition occurs to a highly magnetized state. At the opposite end of the series, $MnNb_2O_6$ behaves like a typical isotropic antiferromagnet. For intermediate compositions, an enhanced response to the applied field is observed as the Fe content rises. This is less noticeable at higher temperatures, as exemplified in Fig. 6(b) for $x = 0.4$. On the other hand, the absence of saturation at fields as high as 10 T may be attributed to the existence of competing FM and AF interactions within the chains.

3.3. Specific-heat measurements

The occurrence of a magnetic transition at low temperature for the $Mn_xFe_{1-x}Nb_2O_6$ compounds was also checked through specific-heat measurements, carried out to temperatures as low as 1.8 K. Fig. 7 shows the concentration dependence of the specific–heat

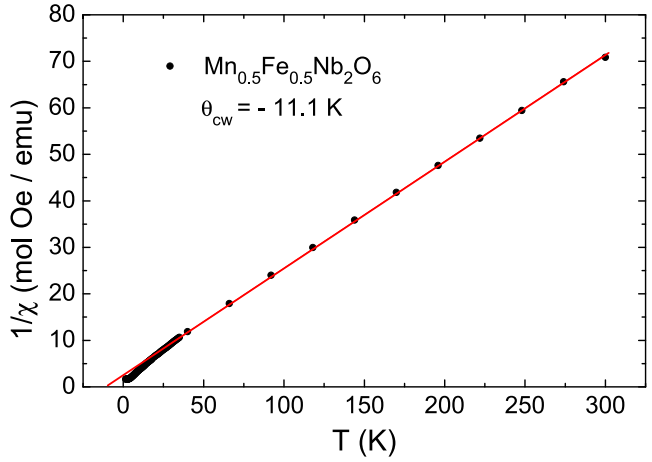

Fig. 4. Inverse of susceptibility and fitting with the Curie-Weiss law for $Mn_{0.5}Fe_{0.5}Nb_2O_6$ sample.

Table 2
Néel temperature, Curie-Weiss temperature, Curie constant (*measured in emu K/mol Oe), and effective magnetic moment of $Mn_xFe_{1-x}Nb_2O_6$ compounds obtained from measurements of dc susceptibility.

x	T_N (K)	θ_{CW} (K)	C (*)	μ_{eff} (μ_B)
1.0	4.4	−24.5	4.78	6.2
0.8	2.4	−19.5	4.61	6.1
0.6	–	−14.3	4.45	6.0
0.5	–	−11.1	4.36	5.9
0.4	–	−7.0	4.29	5.9
0.2	–	−2.1	4.18	5.8
0.0	4.3	8.9	4.08	5.7

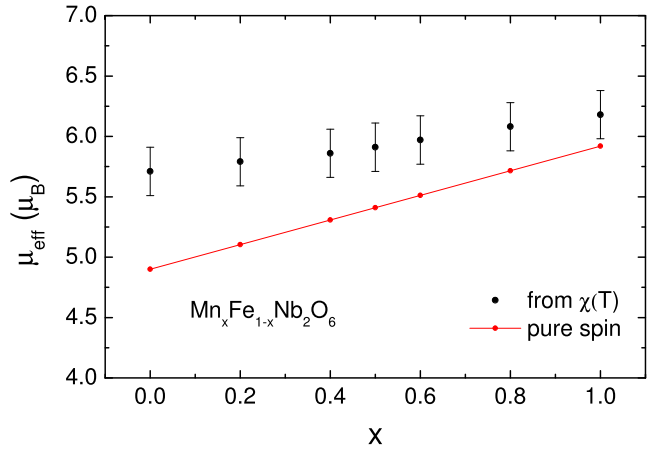

Fig. 5. Experimental values of magnetic moment for $Mn_xFe_{1-x}Nb_2O_6$ compounds and comparison line considering the extreme case of pure spin moment ($g = 2$).

behavior with temperature, including a comparison with the isostructural non-magnetic compound $ZnNb_2O_6$. Clearly defined specific-heat maxima are seen only for the end-member compounds $x = 0$ and 1. The temperature at which the maximum occurs for $x = 1$ agrees well with the T_N value obtained from susceptibility measurements (Table 2). However, for $x = 0$ the maximum is displaced to a higher temperature. This can be due to an underestimation of T_N from the susceptibility, since the measuring magnetic field was nearly half the critical spin-flip value, which means that the transition temperature was somewhere between

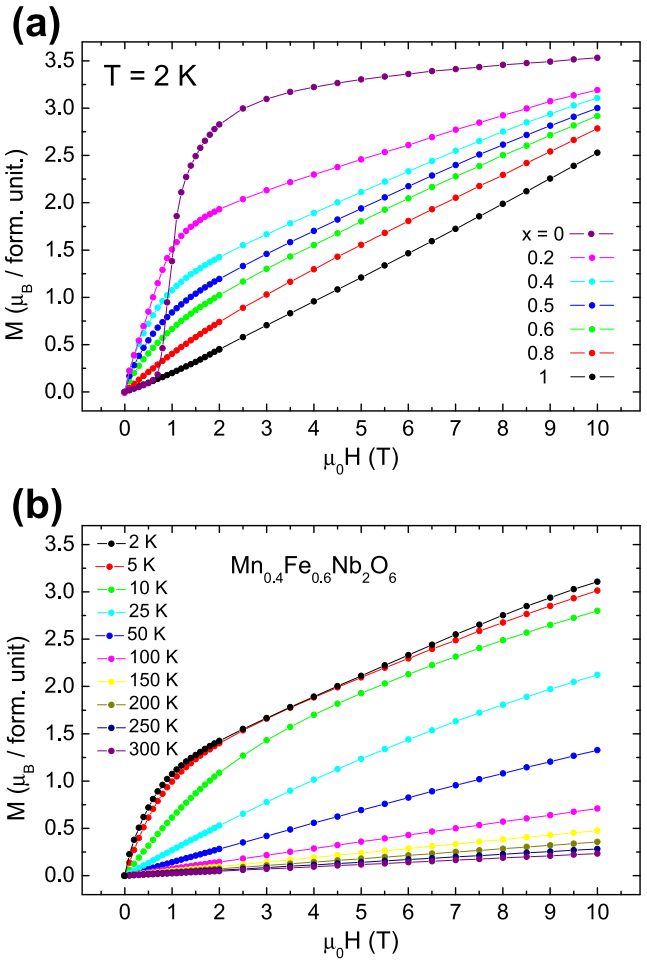

Fig. 6. (a) Isothermal magnetization curves recorded at 2K for the $Mn_xFe_{1-x}Nb_2O_6$ compounds and (b) at the indicated temperatures for $Mn_{0.4}Fe_{0.6}Nb_2O_6$.

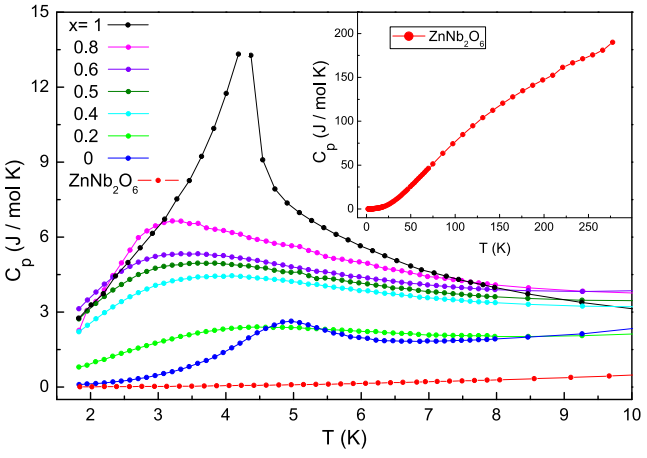

Fig. 7. Comparison of specific–heat behavior of $Mn_xFe_{1-x}Nb_2O_6$ and $ZnNb_2O_6$ (non-magnetic) at low temperatures. The inset shows signal obtained for a non-magnetic $ZnNb_2O_6$ sample.

the true ($H = 0$) T_N and the temperature associated to the spin-flip tricritical point.

3.4. Neutron diffraction

Neutron-diffraction measurements were performed at both 1.5 and 20 K on all samples. An example of Rietveld refinement of the

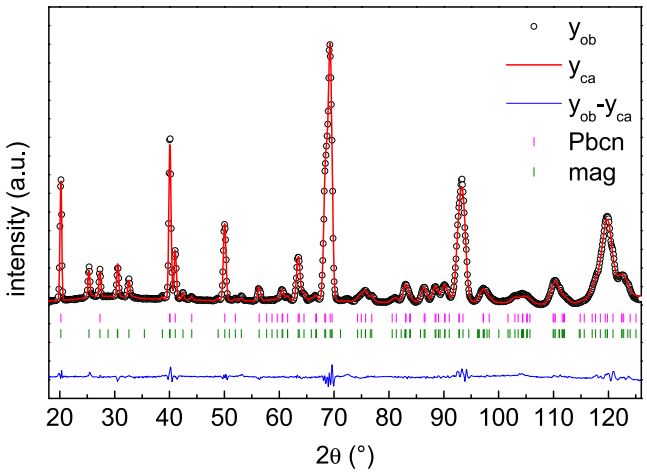

Fig. 8. Rietveld refinement of the ND pattern recorded at 1.5 K for $Mn_{0.8}Fe_{0.2}Nb_2O_6$. The row of markers refers to Bragg-peak positions corresponding to the nuclear and magnetic contributions according to Pbcn space group ($\lambda = 2.52$ Å).

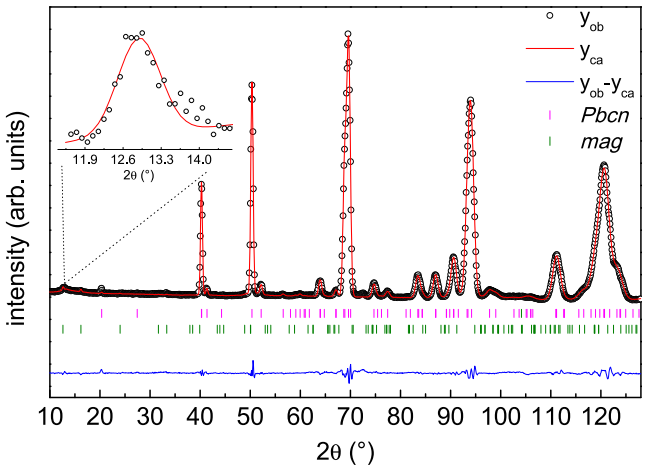

Fig. 9. Rietveld refinement of the ND pattern recorded at 1.5 K for $Mn_{0.2}Fe_{0.8}Nb_2O_6$. The row of markers refers to Bragg-peak positions corresponding to the nuclear and magnetic contributions according to Pbcn space group ($\lambda = 2.52$ Å). The inset shows the broader magnetic peak.

ND pattern ($\lambda = 2.52$ Å) is shown in Fig. 8 for the $x = 0.8$ sample at 1.5 K. All the observed Bragg positions were found to correspond to the *Pbcn* space group typical of the Columbite structure. The magnetic structure observed at this temperature is commensurate with the lattice and presents a propagation vector $\mathbf{k} = (0, 0, 0)$, with two interpenetrating sublattices of opposite spins. Cell parameters determined with this kind of refinement are listed in Table 3 for three representative samples: pure $MnNb_2O_6$ compared with low and high Fe substitutions. Fitting-quality factors are also quoted. The cell parameters obtained in this work, both from XRD (Table 1) and ND (Table 3), are in agreement with the literature [2,17].

For $Mn_{0.2}Fe_{0.8}Nb_2O_6$, the neutron diffraction pattern recorded for at 1.5 K shows magnetic peaks broader than the nuclear ones (Fig. 9). So, the Lorentzian peak-broadening Γ coefficients for the two sets of reflections were varied independently. A mean correlation length for the magnetic order was estimated as $\xi = K\lambda/\Delta\Gamma$ where K is the Scherrer constant (0.9) [8]. The excess Lorentzian broadening $\Delta\Gamma$ was calculated as the difference between Γ's for magnetic (7.9 mrad) and nuclear (4.8 mrad) reflections, assuming the latter to be limited by instrumental resolution. The estimated magnetic coherence length thus determined for this sample is 826 ± 80 Å. The magnetic peak localized at $2\theta = 12.6°$ agrees with a magnetic order with propagation vector $\mathbf{k} = (0, \frac{1}{2}, 0)$, the same observed for $FeNb_2O_6$.

In agreement with the magnetic susceptibility results, shown in Table 2, ND measurements confirm the absence of a magnetic order for temperatures as low as 1.5 K for the $x = 0.4$, 0.5, and 0.6 compositions. However, the difference pattern obtained by subtracting the diffraction pattern recorded at 20 K from that recorded at 1.5 K exhibits a broad bump which we associate with short-range magnetic order. As an example, the left panel of Fig. 10 shows the ND pattern for $Mn_{0.4}Fe_{0.6}Nb_2O_6$, highlighting the region where a magnetic diffuse signal is clearly visible.

Table 3
Structural parameters, quality factors, and magnetic moments obtained from Rietveld refinement of the ND pattern recorded at the indicated temperatures for $Mn_xFe_{1-x}Nb_2O_6$ compounds. The $x = 0.2$ sample does not present truly long-range order at 1.5 K. Its magnetic moment was estimated from relatively broad peaks, as explained in the text.

		$MnNb_2O_6$		$Mn_{0.8}Fe_{0.2}Nb_2O_6$		$Mn_{0.2}Fe_{0.8}Nb_2O_6$	
Temperature		20 K	1.5 K	20 K	1.5 K	20 K	1.5 K
	x	0	0	0	0	0	0
Mn/Fe	y	0.186(4)	0.165(3)	0.205(9)	0.189(6)	0.164(2)	0.156(2)
	z	0.25	0.25	0.25	0.25	0.25	0.25
	x	0.1605(5)	0.1600(4)	0.1609(4)	0.1610(4)	0.1723(6)	0.1612(5)
Nb	y	0.316(2)	0.315(1)	0.318(1)	0.3198(9)	0.317(1)	0.314(1)
	z	0.763(3)	0.763(2)	0.758(2)	0.757(2)	0.746(2)	0.747(2)
	x	0.0945(7)	0.0954(6)	0.0969(5)	0.0973(5)	0.0832(6)	0.0958(6)
O1	y	0.394(2)	0.400(2)	0.400(2)	0.400(2)	0.380(1)	0.399(2)
	z	0.434(2)	0.438(2)	0.431(2)	0.432(2)	0.416(2)	0.422(2)
	x	0.0803(7)	0.0817(6)	0.0820(5)	0.0820(4)	0.0710(5)	0.0825(4)
O2	y	0.107(2)	0.109(2)	0.112(2)	0.112(2)	0.109(3)	0.120(2)
	z	0.907(3)	0.902(2)	0.905(2)	0.904(2)	0.893(2)	0.897(2)
	x	0.2577(9)	0.2541(7)	0.2564(7)	0.2564(6)	0.2602(8)	0.258(1)
O3	y	0.128(2)	0.128(2)	0.128(2)	0.128(1)	0.115(2)	0.120(3)
	z	0.586(3)	0.585(2)	0.584(2)	0.584(2)	0.565(2)	0.574(3)
a (Å)		14.428(2)	14.414(2)	14.397(2)	14.397(2)	14.296(2)	14.280(6)
b (Å)		5.7635(1)	5.7571(6)	5.7583(7)	5.7580(5)	5.7374(4)	5.7313(4)
c (Å)		5.0823(1)	5.0775(5)	5.0761(5)	5.0754(5)	5.0505(2)	5.044(5)
Volume (Å^3)		422.6(2)	421.35(9)	420.84(7)	420.76(8)	414.27(7)	412.88(6)
R_{wp} (%)		5.3	4.5	3.9	3.7	3.0	2.6
R_B (%)		7.2	6.4	4.1	4.1	2.9	1.5
R_M (%)		–	9.4	–	17.7	–	–
$\mu(\mu_B)$		–	4.13(6)	–	2.26(7)	–	0.9(1)

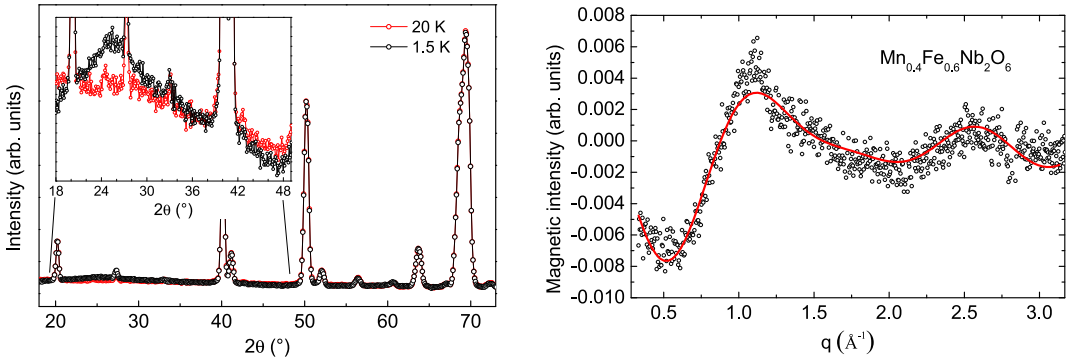

Fig. 10. Left: ND patterns recorded at 20 K and 1.5 K for $Mn_{0.4}Fe_{0.6}Nb_2O_6$, with the inset showing an enlarged view of the region in which a diffuse scattering of magnetic origin is observed. Right: Detailed view of the diffuse neutron-scattering data, and fitting using Eq. (2).

A similar case has been recently reported for the $Ni_xFe_{1-x}Nb_2O_6$ and $Fe_xCo_{1-x}Nb_2O_6$ series [12,14]. Antiferromagnetic short-range order contributes to the specific heat anomaly. As a consequence, the Schottky anomaly observed in the specific heat is shifted down in temperature around 2 to 3 K, becoming broader and lower. There is a clear increase in the specific heat, but it is not sharp enough to characterize a magnetic phase transition (long range order), which is consistent with the absence of magnetic neutron-diffraction peaks.

Short-range spin-spin correlations give rise to magnetic scattering whose signal strength is usually described by an expression first proposed for spin glasses [29,30], later applied to pyrochlores [31–33], and more recently also to ANb_2O_6-type samples [12]. The signal intensity is given by

$$I(q) = N\left[\frac{1}{2}r_0\gamma_0 f_m(q)\right]^2 \frac{2}{3}\sum_{i=1}^{n} c_i\gamma_i \frac{\sin(qR_i)}{qR_i}, \quad (1)$$

where $\frac{1}{2}r_0\gamma_0$ represents the scattering length per Bohr magneton, $f_m(q)$ is the magnetic form factor of the mean $(Mn/Fe)^{2+}$ cation, the summation is over coordination shells surrounding a central atom, c_i and R_i are, respectively, the number of neighbors and the radius of the coordination shell, known from crystallographic data, and γ_i is the average spin correlation at each bond distance. For the $Mn_xFe_{1-x}Nb_2O_6$ compounds, we took into account distances up to 7.70 Å, which corresponds approximately to the fifth neighbor. Then we fitted the data in the bump region through the following simplified equation

$$I(q) = \sum_{i=1}^{n} c_i\Gamma_i \frac{\sin(qR_i)}{qR_i} + B, \quad (2)$$

where Γ_i and B are adjustable parameters. The Γ_i coefficient is proportional to the average spin-spin correlation function for each interatomic distance, absorbing all the coefficients in Eq. (1), and B is a constant background contribution. The right panel of Fig. 10 shows the fitted curve (smooth line) superposed to the signal for $x = 0.4$. The extracted values of spin-spin correlations are summarized in Table 4.

The typical correlation distances shown in Table 4 and also in Fig. 11 present very small variations with composition. Columns 2 and 3 of Table 4 clearly indicate that AF interactions are dominant within a zig-zag chain for these intermediate concentrations of the Fe/Mn solid solution. A sign change is seen for spin correlations between first and second neighbors along the same chain, corresponding to the distances 3.16 and 5.06 Å, which is consistent with a simple AF ordering in the chain. It is also noticeable that the absolute value of relative correlations grow with the Mn fraction (columns 2 to 4 in Table 4). This behavior may be interpreted as

Table 4
Comparison of magnetic correlations at increasing average cation distances (R_i) for three compositions of $Mn_xFe_{1-x}Nb_2O_6$, as derived from fitting Eq. (2) to the neutron diffuse-scattering signal. The correlation strength is normalized to its shortest-distance value for the $x = 0.5$ sample.

x	Spin-spin correlations				
0.4	−0.59	−1.56	0.76	0.62	0.14
0.5	−1	−1.99	0.99	1.15	0.16
0.6	−1.51	−2.44	1.08	1.77	0.14
R_i (Å)	3.16	4.61	5.06	5.74	7.70

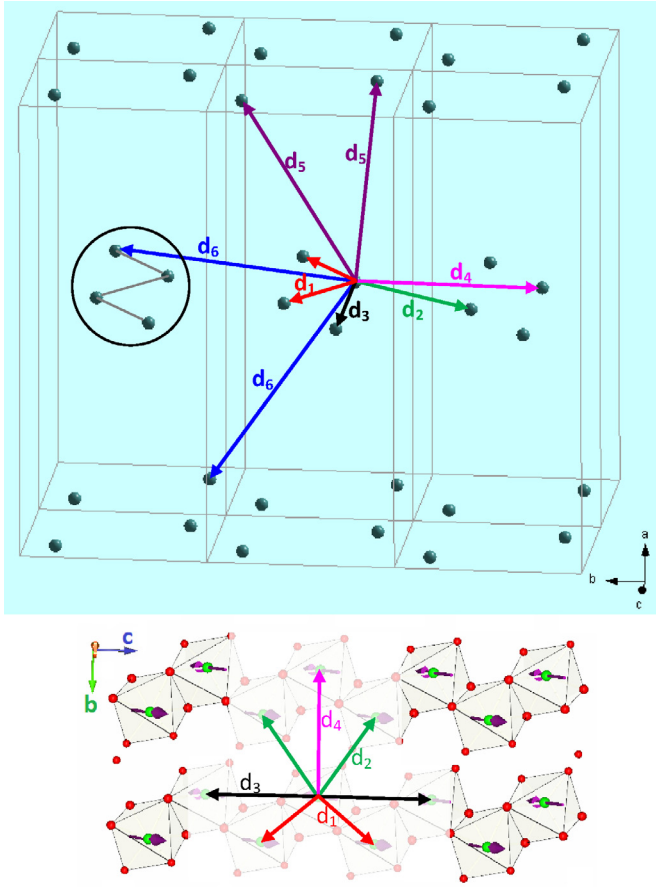

Fig. 11. Shortest inter atomic distances between magnetic ions involved in the magnetic interactions and taken into account in the analysis of the diffuse neutron scattering.

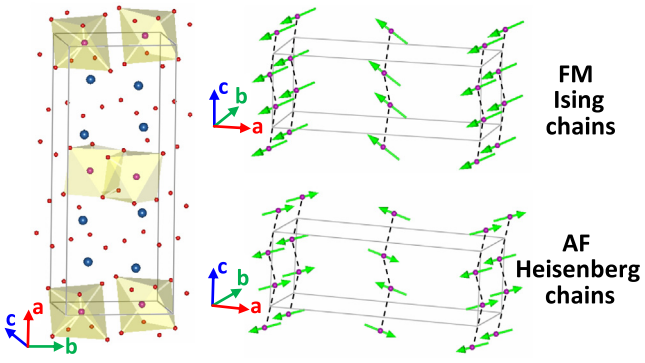

Fig. 12. Left: Crystal structure displaying the octahedra around the Fe/Mn magnetic cations. Right: Comparison of the magnetic structures observed for the extreme composition of $Mn_xFe_{1-x}Nb_2O_6$, the ferromagnetic Ising chains ($x = 0$) and the antiferromagnetic Heisenberg chains ($x = 1$).

a strengthening of magnetic correlations for larger Mn concentration, in agreement with the observed increase of θ_{CW} (Table 2). The intermediate distance (4.61 Å) is related to AF interchain shortest-distance correlations. In contrast, for cations having the same x and z coordinates in neighboring chains (same zig or same zag), at 5.74 Å, the observed correlations are ferromagnetic. The last shell in Table 4 involves both intra- and interchain contributions, and corresponds to averages over a large number of atoms. The sequence of short-distance correlations observed in Table 4 is consistent with the magnetic pattern of the pure-Mn Columbite $MnNb_2O_6$ [16]. Fig. 12 shows the crystal structure of the $Mn_xFe_{1-x}Nb_2O_6$ compounds, showing the oxygen octahedra chains surrounding the Mn atoms and the magnetic arrangements, AF Heisenberg chains corresponds to $x = 1$ and FM Ising type chains to $x = 0$.

4. Conclusions

In this work, we presented a systematic study of $Mn_xFe_{1-x}Nb_2O_6$ samples in the whole composition range. X-ray diffraction reveals a single phase of *Pbcn* symmetry throughout the entire solid solution, with cell parameters varying linearly with x, following Vegard's law. The measured magnetic susceptibility as a function of temperature shows a broad maximum, characteristic of low dimensional magnetic behavior, followed by an inflection point (T_N) for samples with $x = 1.0$, 0.8, and 0, for which long-range AF order occurs below Néel temperatures of 4.4, 2.4 K, and 4.3 K, respectively. Curie-Weiss fitting for samples with $x \neq 0$ gives negative Weiss temperatures, characteristic of dominant antiferromagnetic interactions. The isothermal magnetization of these samples varies linearly with applied magnetic field at high temperatures, and do not show any metamagnetic transitions for $T < T_N$ at applied fields up to 10 T. In contrast, the Curie-Weiss temperature of $FeNb_2O_6$ is positive, and a metamagnetic transition is seen at $\mu_0 H = 0.95$ T, at $T = 2$ K, as previously reported [14], and can be interpreted as resulting from a spin-flip of ferromagnetic chains that are antiferromagnetically coupled to yield the ordered phase. Samples with low to intermediate Mn content do not show long-range magnetic order. For these, short-range correlations revealed from neutron diffuse scattering showed dominant antiferromagnetic interactions with nearest neighbors and ferromagnetic correlations with the next ones in the same chain.

One of the main points worth noticing from our results is the strong instability of ferromagnetic chains in this quasi-one-dimensional system against substitution of Mn for Fe. The exchange interactions become dominantly antiferromagnetic already at high temperatures, and the low-temperature AF ordering is essentially three-dimensional, in contrast to the FM chains observed for Fe, Co, and Ni cations in the same family of compounds [14,12]. This indicates that AF exchange coupling occurs not only between Mn ions but also between Mn and Fe. It also opens the prospect of investigating whether this same effect would be observed with Mn substitution in Co or Ni chains.

Acknowledgments

Funding for this project was provided by a grant from Région Rhône-Alpes (MIRA scholarship). The present work was also supported by the Brazilian agency CNPq, and in part by the Brazilian-France agreement CAPES-COFECUB (No. 600/08). The Institute Laue Langevin and the CNRS are warmly acknowledged for providing the neutron facility.

Appendix A. Supplementary data

Supplementary data associated with this article can be found, in the online version, at https://doi.org/10.1016/j.jmmm.2018.02.011.

References

[1] C. Heid, H. Weitzel, P. Burlet, M. Winkelmann, H. Ehrenberg, H. Fuess, Magnetic phase diagrams of $CoNb_2O_6$, Phys. B 234–236 (1997) 574–575, https://doi.org/10.1016/S0921-4526(96)01189-1, proceedings of the First European Conference on Neutron Scattering.
[2] O.V. Nielsen, B. Lebech, F.K. Larsen, L.M. Holmes, A.A. Ballman, A neutron diffraction study of the nuclear and magnetic structure of $MnNb_2O_6$, J. Phys. C: Solid State Phys. 9 (12) (1976) 2401, https://doi.org/10.1088/0022-3719/9/12/023.
[3] I. Yaeger, A. Morrish, C. Boumford, C. Wong, B. Wanklyn, B. Garrard, Low-temperature Mössbauer studies of $FeNb_2O_6$, Solid State Commun. 28 (8) (1978) 651–653, https://doi.org/10.1016/0038-1098(78)90600-2.
[4] Y. Zhou, M. Lü, Z. Qiu, A. Zhang, Q. Ma, H. Zhang, Z. Yang, Photoluminescence of $NiNb_2O_6$ nanoparticles prepared by combustion method, Mater. Sci. Eng., B 140 (1–2) (2007) 128–131, https://doi.org/10.1016/j.mseb.2007.04.002.
[5] R.C. Pullar, C. Vaughan, N.M. Alford, The effects of sintering aids upon dielectric microwave properties of columbite niobates, $M^{2+}Nb_2O_6$, J. Phys. D: Appl. Phys. 37 (3) (2004) 348, https://doi.org/10.1088/0022-3727/37/3/006.
[6] R.C. Pullar, The synthesis, properties, and applications of columbite niobates ($M^{2+}Nb_2O_6$): a critical review, J. Am. Ceram. Soc. 92 (3) (2009) 563–577, https://doi.org/10.1111/j.1551-2916.2008.02919.x.
[7] E.J. Kinast, V. Antonietti, D. Schmitt, O. Isnard, J.B.M. da Cunha, M.A. Gusmão, C. A. dos Santos, Bicriticality in $Fe_xCo_{1-x}Ta_2O_6$, Phys. Rev. Lett. 91 (19) (2003) 197208, https://doi.org/10.1103/PhysRevLett. 91.197208.
[8] S.A.J. Kimber, J.P. Attfield, Disrupted antiferromagnetism in the brannerite Mnv_2o_6, Phys. Rev. B 75 (2007), https://doi.org/10.1103/PhysRevB.75.064406, 064406.
[9] Z. Chuan-Cang, L. Fa-Min, D. Peng, C. Lu-Gang, Z. Wen-Wu, Z. Huan, Synthesis, structure and antiferromagnetic behaviour of brannerite MnV_2O_6, Chin. Phys. B 19 (6) (2010), https://doi.org/10.1088/1674-1056/19/6/067503, 067503.
[10] C. Calvo, D. Manolescu, Refinement of the structure of CuV_2O_6, Acta Crystallogr., Sect. B 29 (8) (1973) 1743–1745, https://doi.org/10.1107/S0567740873005455.
[11] G. Blasse, Qualitative approach to the structural differences between some mixed metal oxides containing Sb^{+5}, Nb^{+5} and Ta^{+5}, J. Inorg. Nucl. Chem. 26 (7) (1964) 1191–1199, https://doi.org/10.1016/0022-1902(64)80199-8.
[12] P.W.C. Sarvezuk, M.A. Gusmão, J.B.M. da Cunha, O. Isnard, Magnetic behavior of the $Ni_xFe_{1-x}Nb_2O_6$ quasi-one-dimensional system: isolation of Ising chains by frustration, Phys. Rev. B 86 (2012), https://doi.org/10.1103/PhysRevB.86.054435, 054435.
[13] P.W.C. Sarvezuk, E.J. Kinast, C.V. Colin, M.A. Gusmão, J.B.M. da Cunha, O. Isnard, New investigation of the magnetic structure of $CoNb_2O_6$ columbite, J. Appl. Phys. 109 (7) (2011), https://doi.org/10.1063/1.3562516, 07E160.
[14] P.W.C. Sarvezuk, E.J. Kinast, C.V. Colin, M.A. Gusmão, J.B.M. da Cunha, O. Isnard, Suppression of magnetic ordering in quasi-one-dimensional $Fe_xCo_{1-x}Nb_2O_6$ compounds, Phys. Rev. B 83 (17) (2011) 174412, https://doi.org/10.1103/PhysRevB.83.174412.
[15] S. Kobayashi, S. Mitsuda, M. Ishikawa, K. Miyatani, K. Kohn, Three-dimensional magnetic ordering in the quasi-one-dimensional Ising magnet $CoNb_2O_6$ with partially released geometrical frustration, Phys. Rev. B 60 (1999) 3331–3345, https://doi.org/10.1103/PhysRevB.60.3331.
[16] M.L. Hneda, J.B.M. da Cunha, M.A.C. Gusmão, O. Isnard, Low dimensional magnetism in $MnNb_{2-x}V_xO_6$, Mater. Res. Bull. 74 (2016) 169–176, https://doi.org/10.1016/j.materresbull.2015.10.030.

[17] L. Holmes, A. Ballman, R. Hecker, Antiferromagnetic ordering in $MnNb_2O_5$ studied by magnetoelectric and magnetic susceptibility measurements, Solid State Commun. 11 (3) (1972) 409–413, https://doi.org/10.1016/0038-1098(72)90020-8.

[18] D. Prabhakaran, F. Wondre, A. Boothroyd, Preparation of large single crystals of ANb_2O_6 (A = Ni Co, Fe, Mn) by the floating-zone method, J. Cryst. Growth 250 (1–2) (2003) 72–76, https://doi.org/10.1016/S0022-0248(02)02229-7, proceedings of the Fourteenth American Conference on Crystal Grow th and Epitaxy.

[19] I. Yaeger, A.H. Morrish, B.M. Wanklyn, B.J. Garrard, Magnetization studies in transition-metal niobates. II. $FeNb_2O_6$, Phys. Rev. B 16 (1977) 2289–2299, https://doi.org/10.1103/PhysRevB.16.2289.

[20] R. Coldea, D.A. Tennant, E.M. Wheeler, E. Wawrzynska, D. Prabhakaran, M. Telling, K. Habicht, P. Smeibidl, K. Kiefer, Quantum criticality in an Ising chain: experimental evidence for emergent e8 symmetry, Science 327 (5962) (2010) 177–180, https://doi.org/10.1126/science.1180085.

[21] S. Lee, R.K. Kaul, L. Balents, Interplay of quantum criticality and geometric frustration in columbite, Nat. Phys. 6 (9) (2010) 702–706, https://doi.org/10.1038/nphys1696.

[22] J.A. Kjäll, F. Pollmann, J.E. Moore, Bound states and E_8 symmetry effects in perturbed quantum Ising chains, Phys. Rev. B 83 (2011), https://doi.org/10.1103/PhysRevB.83.020407, 020407.

[23] A.W. Kinross, M. Fu, T.J. Munsie, H.A. Dabkowska, G.M. Luke, S. Sachdev, T. Imai, Evolution of quantum fluctuations near the quantum critical point of the transverse field Ising chain system $CoNb_2O_6$, Phys. Rev. X 4 (2014), https://doi.org/10.1103/PhysRevX.4.031008, 031008.

[24] I. Cabrera, J.D. Thompson, R. Coldea, D. Prabhakaran, R.I. Bewley, T. Guidi, J.A. Rodriguez-Rivera, C. Stock, Excitations in the quantum paramagnetic phase of the quasi-one-dimensional Ising magnet $CoNb_2O_6$ in a transverse field: Geometric frustration and quantum renormalization effects, Phys. Rev. B 90 (2014), https://doi.org/10.1103/PhysRevB.90.014418, 014418.

[25] S.C. Tarantino, M. Zema, F. Maglia, M.C. Domeneghetti, M.A. Carpenter, Structural properties of $Mn_{1-x}Fe_xNb_2O_6$ columbites from X-ray diffraction and IR spectroscopy, Phys. Chem. Miner. 32 (8) (2005) 568–577, https://doi.org/10.1007/s00269-005-0031-4.

[26] J. Rodrguez-Carvajal, Recent advances in magnetic structure determination by neutron powder diffraction, Physica B 192 (1–2) (1993) 55–69, https://doi.org/10.1016/0921-4526(93)90108-I.

[27] L.B. McCusker, R.B. Von Dreele, D.E. Cox, D. Louër, P. Scardi, Rietveld refinement guidelines, J. Appl. Crystallogr. 32 (1) (1999) 36–50, https://doi.org/10.1107/S0021889898009856.

[28] F. Garca-Alvarado, A. Orera, J. Canales-Vzquez, J.T.S. Irvine, On the electrical properties of synthetic manganocolumbite $MnNb_2O_{6-\delta}$, Chem. Mater. 18 (16) (2006) 3827–3834, https://doi.org/10.1021/cm0603203.

[29] E. Bertaut, P. Burlet, Ordre magnetique a courte distance dans les solutions solides $Mn_xCr_{1-x}S$, Solid State Commun. 5 (4) (1967) 279–283, https://doi.org/10.1016/0038-1098(67)90273-6.

[30] A. Wiedenmann, P. Burlet, H. Scheuer, P. Convert, Spin correlation in the quasi-1D spin glass $FeMgBO_4$, Solid State Commun. 38 (2) (1981) 129–133, https://doi.org/10.1016/0038-1098(81)90804-8.

[31] J.E. Greedan, J.N. Reimers, C.V. Stager, S.L. Penny, Neutron-diffraction study of magnetic ordering in the pyrochlore series $R_2Mo_2O_7$ (R = Nd, Tb, Y), Phys. Rev. B 43 (1991) 5682–5691, https://doi.org/10.1103/PhysRevB.43.5682.

[32] J.E. Greedan, J.N. Reimers, S.L. Penny, C.V. Stager, Short range ordering in a three dimensionally frustrated magnet, $Tb_2Mo_2O_7$, by wide and small angle neutron diffraction, J. Appl. Phys. 67 (9) (1990) 5967–5969, https://doi.org/10.1063/1.346030.

[33] I. Mirebeau, A. Apetrei, J. Rodŕguez-Carvajal, P. Bonville, A. Forget, D. Colson, V. Glazkov, J.P. Sanchez, O. Isnard, E. Suard, Ordered Spin Ice State and Magnetic Fluctuations in $Tb_2Sn_2O_7$, Phys. Rev. Lett. 94 (2005) 246402, https://doi.org/10.1103/PhysRevLett. 94.246402.